THE JOURNAL OF BIOLOGICAL CHEMISTRY VOL. 292, NO. 8, pp. 3506–3516, February 24, 2017

Intramembrane Proteolysis of Astrotactins*[S]

Received for publication, November 14, 2016, and in revised form, January 14, 2017 Published, JBC Papers in Press, January 18, 2017, DOI 10.1074/jbc.M116.768077

Hao Chang[‡1], **Philip M. Smallwood**[‡], **John Williams**[‡], **and Jeremy Nathans**[‡§¶2]

From the Departments of [‡]*Molecular Biology and Genetics,* [§]*Neuroscience, and* [¶]*Ophthalmology, Howard Hughes Medical Institute, Johns Hopkins University School of Medicine, Baltimore, Maryland 21205*

Edited by Paul E. Fraser

Astrotactins are vertebrate-specific membrane proteins implicated in neuron-glia interactions during central nervous system development and in hair follicle polarity during skin development. By studying epitope-tagged derivatives of mouse astrotactin-2 (Astn2) produced in transfected cells, we determined that the amino and carboxyl termini reside in the extracellular space and are initially linked by two transmembrane segments and a single cytoplasmic domain. We further show that Astn2 undergoes proteolytic cleavage in the second transmembrane domain (TM2) and that a disulfide bond holds the resulting two fragments together. Recombinant Astn1 also undergoes TM2 cleavage, as does Astn2 isolated from mouse cerebellum. Astn2 intramembrane proteolysis is insensitive to replacement of TM2 by the transmembrane domain of CD74 or by 21 alanines. However, replacement of TM2 by the transmembrane domain of CD4, the asialoglycoprotein receptor, or the transferrin receptor eliminates intramembrane proteolysis, as does leucine substitution of residues that overlap or are immediately upstream of the cleavage site. Replacement of the transmembrane domain of CD74 or the asialoglycoprotein receptor with Astn2 TM2 leads to the appearance of a carboxyl-terminal fragment consistent with intramembrane proteolysis. These experiments define a highly unusual transmembrane topology for the astrotactins, reveal intramembrane proteolysis as a feature of astrotactin maturation, and constrain the substrate sequences that are permissive for cleavage of one type 2 transmembrane segment.

Intramembrane proteolysis is a relatively unusual mode of polypeptide cleavage in which an integral membrane protease recognizes and cleaves a membrane-embedded substrate. At present, there are four known families of intramembrane proteases, and each uses a distinct catalytic mechanism: rhomboid family members are serine proteases, site 2 protease family members are metalloproteases, presenilin/γ-secretase/signal peptide peptidase (SPP)[3] family members are aspartyl proteases, and Rce1 (Ras and a-factor converting enzyme 1) is a glutamyl protease (1–5). Intramembrane proteases are found in all kingdoms of life. In several well studied cases they play critical roles in development (cleavage and activation of epidermal growth factor-like ligands by rhomboid-1 in *Drosophila* and cleavage and release of the intracellular domain of Notch by γ-secretase), homeostasis (cleavage and activation of a tethered transcription factor that controls cholesterol synthesis and uptake by mammalian site-2 protease), and disease (processing of the amyloid-β peptide by γ-secretase).

The SPP family is divided into two subfamilies based on the transmembrane topographies of enzyme and substrate (1, 6). The presenilin/γ-secretase subfamily cleaves transmembrane domains oriented with the carboxyl terminus facing the cytoplasm. By contrast, the SPP subfamily, which includes the SPP and SPP-like (SPPL) enzymes, has the opposite transmembrane topology relative to the presenilin/γ-secretase subfamily. SPP/SPPL subfamily members and the site 2 protease are the only known intramembrane proteases that cleave transmembrane domains that are oriented with the amino terminus facing the cytoplasm (type 2 orientation).

Astn1 (astrotactin-1) and Astn2 (astrotactin-2) are homologous transmembrane proteins that have been implicated in neural development and in the response to CNS injury (7–9). *Astn1* is expressed widely in the CNS, whereas *Astn2* is predominantly expressed in the cerebellum (10). In mice, Astn1 has been implicated in neuronal migration along glial scaffolds during CNS development based on *ex vivo* and gene knockout experiments (7, 11). In humans, copy number variations affecting *ASTN2* have been found in individuals with neurodevelopmental disorders, including autism spectrum disorder, attention deficit hyperactivity disorder, obsessive-compulsive disorder, and schizophrenia (12–14). Astrotactins are also widely expressed in non-CNS tissues, and recent mouse genetic experiments have demonstrated a role for Astn2 in biasing the orientation of hair follicles in the context of impaired planar polarity signaling (15). In particular, both spontaneous and genetically engineered deletions of *Astn2* exon5 produced a recessive genetic modifier of the hair polarity phenotype associated with homozygous knock-out of the planar cell polarity gene *Frizzled6*.

Although the biochemical basis of astrotactin function is unknown, the three-dimensional structure of part of the carboxyl-terminal ectodomain of human ASTN2 has recently been determined, and this structure reveals a perforin-like domain, an EGF-like domain, a fibronectin type III domain, and an annexin-like domain (16). Perforin domains are found in

* This work was supported by the Howard Hughes Medical Institute. The authors declare that they have no conflicts of interest with the contents of this article.

[S] This article contains supplemental Table S1 and Figs. S1–S3.

[1] Present address: Dept. of Dermatology, University of Wisconsin-Madison, 1300 University Ave., Madison, WI 53706.

[2] To whom correspondence should be addressed: 805 PCTB, 725 N. Wolfe St., Johns Hopkins University School of Medicine, Baltimore, MD 21205. Tel.: 410-955-4679; Fax: 410-614-0827; E-mail: jnathans@jhmi.edu.

[3] The abbreviations used are: SPP, signal peptide peptidase; BME, β-mercaptoethanol; IC, intracellular; SP, signal peptide; SPPL, signal peptide peptidase-like; SREBP, sterol regulatory element binding proteins; TM, transmembrane; RIPA, radioimmune precipitation assay.

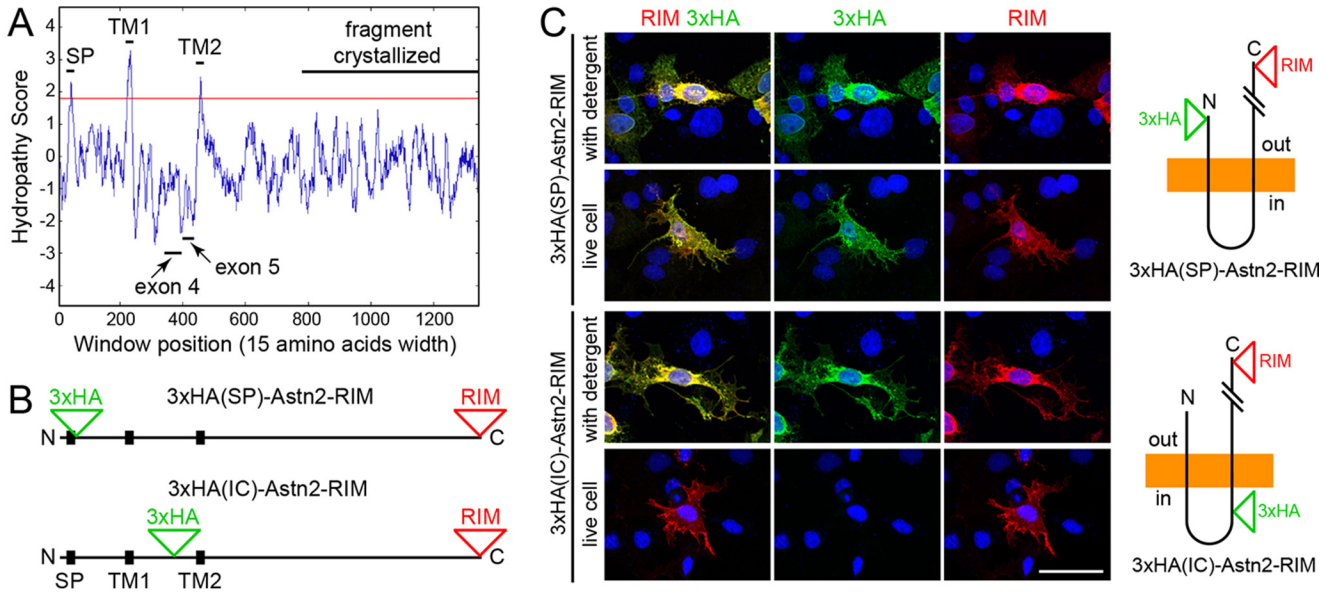

FIGURE 1. **Transmembrane topology of Astn2.** *A*, hydropathy profile of mouse Astn2 determined by the method of Kyte and Dolittle with a 15-amino acid window and showing the locations of the SP, TM1, TM2, exons 4 and 5, and the part of the ASTN2 carboxyl-terminal ectodomain that has been crystallized (16). *B*, linear structures of 3×HA(SP)-Astn2-RIM and 3×HA(IC)-Astn2-RIM aligned to the hydropathy profile in *A*, with hydrophobic regions marked by *black rectangles*. *C*, rabbit anti-3×HA and mouse anti-RIM immunostaining of fixed and detergent-permeabilized or live COS7 cells transfected with 3×HA(SP)-Astn2-RIM or 3×HA(IC)-Astn2-RIM. The panels in the *left column* show merged fluorescent signals; the panels in the *right two columns* show separated fluorescent signals. The two proteins are diagrammed at *right*; *orange* represents the lipid bilayer. *out*, extracellular; *in*, intracellular. *Scale bar* in *C*, 40 μm.

variety of membrane pore-forming proteins, but the structure of the ASTN2 perforin-like domain suggests that it is unlikely to form pores.

In the present work, we have defined the transmembrane topology of mouse Astn2 and shown that this protein undergoes a single intramembrane proteolytic cleavage in the second of two transmembrane segments. The two fragments remain associated via a disulfide bond between a pair of cysteines very close to the amino terminus of each fragment. Intramembrane cleavage is likely mediated by a member of the SPP/SPPL family. The presence of extracellular amino and carboxyl termini together with intramembrane cleavage makes the structure and maturation of astrotactins highly unusual.

Results

Transmembrane Topology of Astrotactins—Recent additions to the publicly available nucleotide databases, together with comparisons between cDNA and genomic DNA among multiple vertebrate species have established the likely amino acid sequences of multiple isoforms of mouse Astn1 and Astn2, with the largest isoforms having predicted lengths of 1302 (REFSEQ, accession no. NM_001205204.1) and 1352 (UniProtKB, accession no. Q80Z10) amino acids, respectively (supplemental Fig. S1). The hydropathy profiles of Astn1 and Astn2 are nearly identical, with each showing three prominent peaks of hydrophobicity, corresponding to a predicted signal peptide, transmembrane segment 1 (TM1), and TM2. Fig. 1*A* shows the hydropathy profile for Astn2.

To experimentally define the transmembrane topology of Astn2, we inserted a RIM epitope tag at the extreme carboxyl terminus and a 3×HA epitope tag either at position 74, 22 amino acids carboxyl-terminal to the predicted site of signal peptide cleavage, or at position 403 at the junction of exons 4 and 5, between the second and third hydrophobic peaks (Fig. 1*B* and supplemental Fig. S1). These tagged proteins are referred to as "3×HA(SP)-Astn2-RIM" and "3×HA(IC)-Astn2-RIM", respectively, where SP stands for signal peptide, and IC stands for intracellular. Immunostaining of transiently transfected COS7 cells showed antibody binding to the carboxyl-terminal RIM tag when cells were stained in the living state or when cells were fixed and detergent-permeabilized (Fig. 1*C*). The 3×HA tag at position 74 was accessible in both intact and detergent-permeabilized cells. In contrast, the 3×HA tag at position 403 was accessible only in permeabilized cells. Identical results were obtained with transfected HEK293T cells (data not shown). Taken together, these data establish the topology of Astn2 as extracellular amino terminus, TM1, intracellular loop, TM2, and extracellular carboxyl terminus. This interpretation is consistent with the presence of multiple extracellular domains (fibronectin, perforin, EGF, and annexin) near the carboxyl terminus. We note that the plasma membrane localization of a readily detectable fraction of the Astn2 (Fig. 1*C*) is at odds with the observations of Wilson *et al.* (10), in which Astn2 accumulation appeared to be limited to internal membranes. Possibly related to this discrepancy, Wilson *et al.* (10) assigned the second peak in the hydropathy profile (TM1) as the amino-terminal signal peptide.

Mature Astrotactins Are Cleaved to Yield a Disulfide-linked Heterodimer—The first clues that Astn2 might be subject to proteolytic processing in or near TM2 came from a comparison of the apparent mobility of alternatively spliced and/or mutant forms lacking the amino acids encoded by exon 4 (52 amino acids), exon 5 (36 amino acids), or both exons 4 and 5 (88 amino acids), which reside in the intracellular loop. (Unless otherwise noted in the text, Astn proteins analyzed in this study were

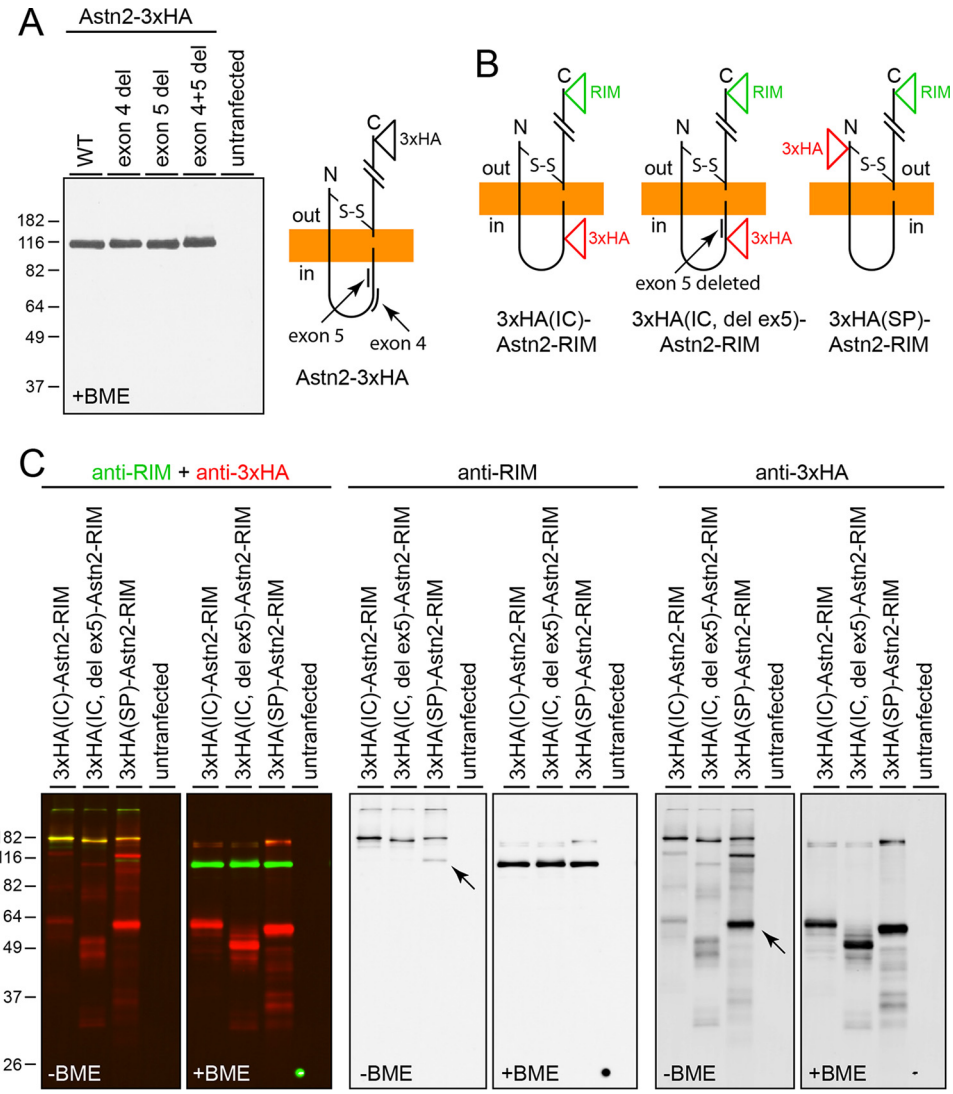

FIGURE 2. **Mature Astn2 consists of two disulfide-linked fragments.** *A*, *left panel*, anti-3×HA immunoblot of Astn2–3×HA variants containing both exons 4 and 5 (WT), or missing exon 4, exon 5, or both exons 4 and 5 produced in HEK293T cells. *Right panel*, diagram of Astn2–3×HA with locations of exons 4 and 5 indicated. Molecular mass markers are at 182, 116, 82, 64, 49, and 37 kDa. *B*, diagrams of 3×HA-Astn2-RIM derivatives analyzed in *C*. *C*, anti-3×HA and anti-RIM immunoblot of the indicated Astn2 derivatives produced in HEK293T cells and treated with or without BME prior to electrophoresis. In this and other figures, the *left panels* show the merged fluorescent immunoblot signals visualized with anti-3×HA and anti-RIM, and the *right panels* show the separated signals. *Arrows* point to the carboxyl-terminal (*left blot*) and amino-terminal (*right blot*) fragments of 3×HA(SP)-Astn2-RIM in the absence of BME. The molecular mass markers in this and other figures are indicated in kDa.

produced in transfected HEK293T cells.) As determined by SDS-PAGE in the presence of β-mercaptoethanol (BME) and immunoblotting for a carboxyl-terminal 3×HA epitope tag, all three variants exhibited the same electrophoretic mobility as the WT control (*i.e.* the isoform containing exons 4 and 5), and this mobility corresponded to a mass of ~115 kDa, which is considerably smaller than the predicted mass of ~150 kDa that corresponds to the unglycosylated polypeptide and its epitope tag (Fig. 2*A*).

To examine this phenomenon in greater detail, we studied double epitope-tagged Astn2 derivatives. Immunoblotting of 3×HA(IC)-Astn2-RIM following SDS-PAGE in the absence of BME revealed a single band of ~180 kDa with both tags (Fig. 2, *B* and *C*). When the same sample was analyzed in the presence of BME, we observed one band of ~55–60 kDa with the 3×HA tag and a second band of ~115 kDa with the RIM tag (Fig. 2, *B* and *C*). These data indicate that mature Astn2 consists of two fragments joined by one or more disulfide bonds. An Astn2 derivative that lacks exon 5 (3×HA(ICdel5)-Astn2-RIM) but is otherwise identical to 3×HA(IC)-Astn2-RIM produces a similar pattern of bands, except that in the presence of BME the amino-terminal fragment has a molecular mass of ~50–55 kDa instead of ~55–60 kDa, which is in reasonable agreement with the calculated decrease of 4.1 kDa because of deletion of exon 5.

3×HA(SP)-Astn2-RIM produced an immunoblot pattern that is similar to that produced by 3×HA(IC)-Astn2-RIM, except for the presence of higher levels of monomeric amino- and carboxyl-terminal fragments in the absence of BME (*arrows* in Fig. 2*C*). This could reflect a partial inhibition of disulfide bond formation by the amino-terminal 3×HA tag, which, as shown below, was inserted eight amino acids distal to one of the disulfide-bonding cysteines (Cys^{66}). In the absence of BME, 3×HA(IC)-Astn2-RIM and 3×HA(ICdel5)-Astn2-RIM exhibit a low level of the monomeric fragments.

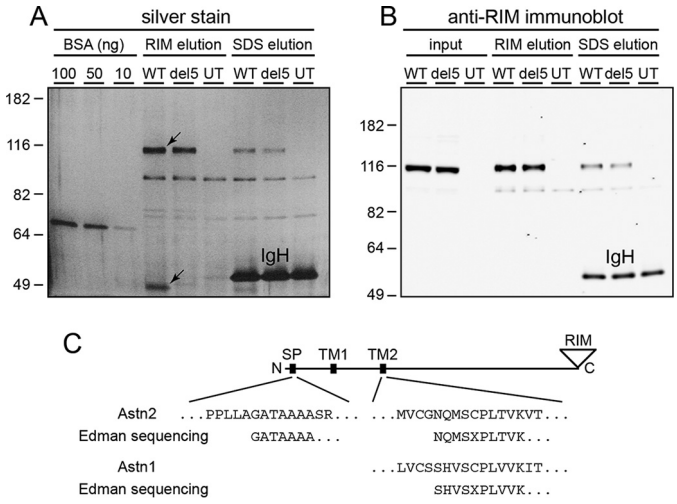

FIGURE 3. **Astn2 signal peptide and Astn1 and Astn2 internal cleavage sites defined by Edman sequencing.** *A*, silver-stained gel showing Rim3F4 immunoaffinity-purified WT and exon 5-deleted variant of Astn2-RIM produced in HEK293T cells. *Arrows* point to amino- and carboxyl-terminal fragments at ~50 and ~115 kDa, respectively. *Left lane*, BSA standards; *center lane*, protein obtained by RIM peptide elution from protein G-Sepharose prebound to mAb Rim3F4 (hereafter "Rim3F4-Sepharose"); *right lane*, protein obtained by subsequent SDS elution from Rim3F4-Sepharose. Molecular mass markers are at 182, 116, 82, 64, and 49 kDa. UT, untransfected HEK293T cells. *IgH*, Rim3F4 heavy chain. The amino-terminal fragment from the exon 5-deleted variant has run off the bottom of the gel. See supplemental Fig. S2 for the same samples run on a higher percentage gel. *B*, anti-RIM immunoblot. *Left lane*, input cell lysate; the *center* and *right lanes* are as described for *A*. The quantities loaded were 1/250 of the input cell lysate (*left lane*) and 1/30 of the RIM-eluted protein (*center lane*); based on quantification the carboxyl-terminal fragment intensities, ~13% of the Astn2 protein was captured. *C*, Astn2 sequence near the carboxyl terminus of the signal peptide and Astn2 and Astn1 sequences in the TM2 region above the aligned amino-terminal Edman sequences from corresponding immunoaffinity-purified polypeptides.

Locating the Astn2 Cleavage Site—To define the site of Astn2 cleavage precisely, Astn2-RIM, produced in transiently transfected HEK293T cells, was immunoaffinity-purified to near homogeneity using immobilized mAb Rim3F4 followed by elution with a RIM epitope peptide (Fig. 3, *A* and *B*; Ref. 17). Following electrophoresis in the presence of BME, a silver stain showed the amino- and carboxyl-terminal Astn2 fragments at approximately equimolar ratio (Fig. 3, *A* and *B*). An analogous purification with an exon 5-deleted version of Astn2-RIM yielded that same carboxyl-terminal fragment and, as expected, a smaller amino-terminal fragment (Fig. 3*A* and supplemental Fig. S2).

Following preparative SDS-PAGE and immunoblotting to PVDF membrane, the amino- and carboxyl-terminal fragments of Astn2-RIM were subjected to amino-terminal (Edman) sequencing. This analysis revealed unique amino termini for each fragment, defining 1) the site of signal peptide cleavage between amino acids Ala^{51} and Gly^{52} that generates the amino terminus of the mature polypeptide and 2) the site of cleavage between amino acids Gly^{465} and Asn^{466} that creates separate amino- and carboxyl-terminal fragments (Figs. 1*A* and 3*C* and supplemental Fig. S1). Interestingly, Gly^{465} and Asn^{466} are predicted to reside within TM2.

Edman sequencing of the carboxyl-terminal fragment of Astn1-RIM showed a unique site of cleavage between Ser^{401} and Ser^{402}, a location that aligns precisely with the Astn2 cleavage site (Fig. 3*C* and supplemental Fig. S1). Thus, Astn1 and Astn2 cleavage in TM2 appears to represent a highly conserved processing event despite the ~50% divergence between Astn1 and Astn2 TM2 amino acid sequences.

Locating the Interchain Disulfide Bond—Based on the primary sequence of Astn2, its transmembrane topology, the TM2 cleavage site, and the three-dimensional structure of a large part of the ectodomain, the identities of the cysteines that could potentially form a disulfide bond between amino- and carboxyl-terminal fragments are highly constrained. The amino-terminal fragment includes three cysteines: Cys^{66}, close to the amino terminus of the mature protein and the only cysteine in the extracellular domain preceding TM1; and Cys^{458} and Cys^{464}, located in TM2, two and eight residues, respectively, from the intramembrane cleavage site (supplemental Fig. S1). We considered the two cysteines in TM2 as unlikely candidates given their predicted intramembrane locations. Moreover, Cys^{464} is not conserved among fish astrotactins.

The carboxyl-terminal fragment of Astn2 has 38 cysteines, and all are conserved across fish, amphibian, avian, and mammalian Astn1 and Astn2 sequences. The most carboxyl-terminal 30 cysteines reside within the Astn2 ectodomain fragment that was crystalized by Ni *et al.* (16), and 16 of these cysteines were observed to form disulfide bonds in the three-dimensional structure (supplemental Fig. S1). The remaining 14 cysteines reside in a part of the polypeptide chain that could not be traced from the electron density map, but it is likely that they form intrachain disulfides because the ectodomain fragment is a monomer in solution (16). Eliminating the most carboxyl-terminal 30 cysteines leaves eight cysteines as potential candidates for participation in interchain disulfide bond formation: Cys^{470}, located five amino acids carboxyl-terminal to the TM2 cleavage site and predicted to reside just within or at the edge of TM2; six cysteines that form a predicted EGF motif with three disulfide bonds; and Cys^{629}, which is not part of a known structural motif. These considerations point to either Cys^{470} or Cys^{629} as the likely partner for Cys^{66}.

To test these predictions, the three likely candidate cysteines for interchain disulfide bond formation were mutated one at a time to serine, and the resulting 3×HA- and RIM-tagged proteins were examined by SDS-PAGE with and without BME. Mutation of Astn2 Cys^{629} to serine resulted in a polypeptide that exhibited an electrophoretic mobility that was indistinguishable from the WT control both in the absence and in the presence of BME (data not shown). In contrast, Fig. 4 shows that mutation of Cys^{66} or Cys^{470} eliminates the ~180-kDa disulfide-linked Astn2 band seen in the WT control in the absence of BME, generating instead an amino-terminal fragment that migrates at the same mobility as the WT amino-terminal fragment and a carboxyl-terminal fragment that migrates at the same mobility (for the C66S mutant) or at slightly reduced mobility (for the C470S mutant) as the WT monomeric carboxyl-terminal fragment. In the presence of BME, the C66S and C470S mutations generate amino- and carboxyl-terminal fragments indistinguishable from those produced by the WT control.

In the absence of BME, the C470S mutant also produces an amino-terminal fragment with an apparent mobility of ~130

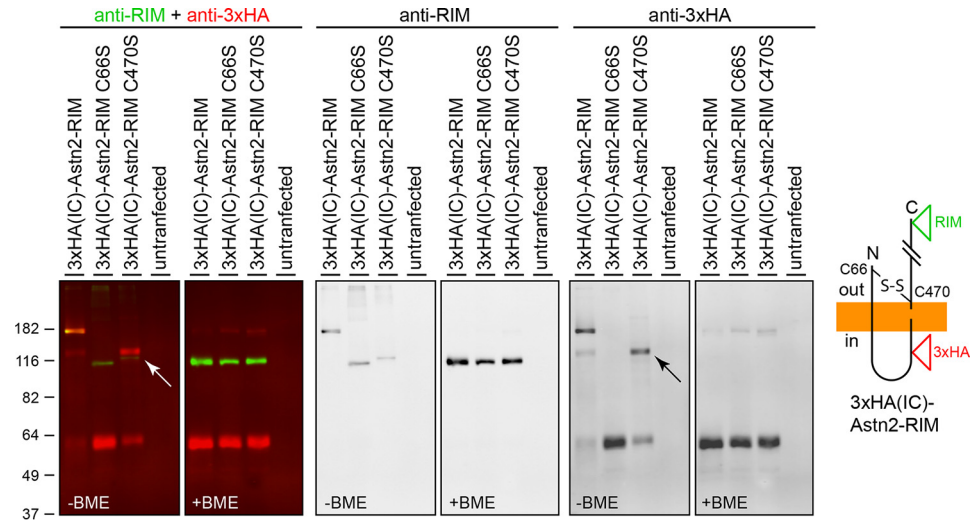

FIGURE 4. **Identifying the cysteines that form the disulfide bond linking amino- and carboxyl-terminal fragments of Astn2.** *Left panel*, anti-RIM and anti-3×HA immunoblots of 3×HA(IC)-Astn2-RIM WT and C66S and C470S Astn2 mutants produced in transfected HEK293T cells. *Arrows* point to the presumptive amino-terminal fragment dimer in the C470S mutant. *Right panel*, diagram of 3×HA(IC)-Astn2-RIM showing the locations of Cys^{66} and Cys^{470}.

kDa, which is accompanied by a reduction in the intensity of the monomeric amino-terminal fragment (*arrows* in Fig. 4). The simplest interpretation of these data is that the ~130-kDa species is a disulfide-linked homodimer of the amino-terminal fragment that forms in the absence of Cys^{470}, presumably by an aberrant Cys^{66}–Cys^{66} bond. We conclude that Cys^{66} in the amino-terminal fragment and Cys^{470} in the carboxyl-terminal fragment represent the two cysteines that form the interchain disulfide that links the two fragments of Astn2 produced by cleavage within TM2. Because these two cysteines are conserved in Astn1 (supplemental Fig. S1), they likely play the same role in the two astrotactins.

Astn2 in Mouse Cerebellum—Having defined the pattern of proteolytic cleavage and interchain disulfide bonding in Astn2 produced in transfected HEK293T cells, we next asked whether native Astn2 exhibits properties consistent with this covalent structure. To enrich Astn2 from a native source, membranes were purified from postnatal day 10 mouse cerebellum, a time and location that *in situ* hybridization has shown to be relatively enriched for Astn2 transcripts (10).

Immunoblotting with antibodies directed at a segment of Astn2 within the extracellular carboxyl terminus revealed the expected BME effect on mobility for 3×HA(IC)-Astn2-RIM produced in HEK293T cells (Fig. 5). In the presence of BME, cerebellum-derived Astn2 showed a slightly faster mobility than HEK293T-derived Astn2, consistent with the presence of the RIM tag at the carboxyl terminus of recombinant Astn2. These data imply an identical or nearly identical point of cleavage in TM2 in native and recombinant Astn2. Most interestingly, in the absence of BME, cerebellum-derived Astn2 exhibited a mobility far lower than the principal band of HEK293T-derived Astn2. These data suggest that, in the cerebellum, the covalent structure of Astn2 includes at least one additional polypeptide linked via a disulfide bond, possibly via Cys^{629} or another cysteine within the Astn2 carboxyl terminus.

Sequence Requirements for TM2 Cleavage—Because Astn TM2 is present in a type 2 orientation (*i.e.* amino terminus facing the cytoplasm), the protease that catalyzes its cleavage

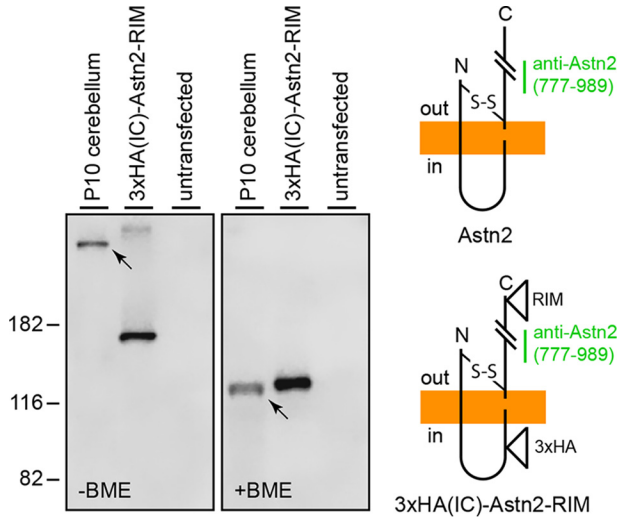

FIGURE 5. **Astn2 processing in mouse cerebellum.** Immunoblots of postnatal day 10 mouse cerebellum membranes and 3×HA(IC)-Astn2-RIM from transfected HEK293T cells treated without BME (*left panel*) and with BME (*right panel*). The gels were run longer than for Figs. 2–4, and the blots were probed with rabbit antibodies raised against amino acids 777–989 of mouse Astn2. *Arrows* indicate the Astn2 bands from mouse cerebellum. *Right panel*, diagrams of native Astn2 (*upper panel*) and 3×HA(IC)-Astn2-RIM (*lower panel*) showing the location of amino acids 777–989 within the carboxyl-terminal fragment, the region that was used for immunization.

is most likely a member of the SPP/SPPL family. Sequence requirements for cleavage by SPP/SPPL family members have been studied with several substrates, revealing a preference for α-helix destabilizing residues in the transmembrane segment and strong modulation by flanking extramembrane sequences (18–20). Aside from these trends, known or presumed SPP/SPPL substrates do not exhibit an obvious consensus at the primary sequence level (1, 6). To address the question of substrate recognition in the context of Astn2 TM2, we initially created a series of alanine block substitutions encompassing all of TM2 and its immediate flanks (Fig. 6*A*). Interestingly, none of the alanine substitutions abolished TM2 cleavage, although many modestly reduced the cleavage efficiency and/or subtly

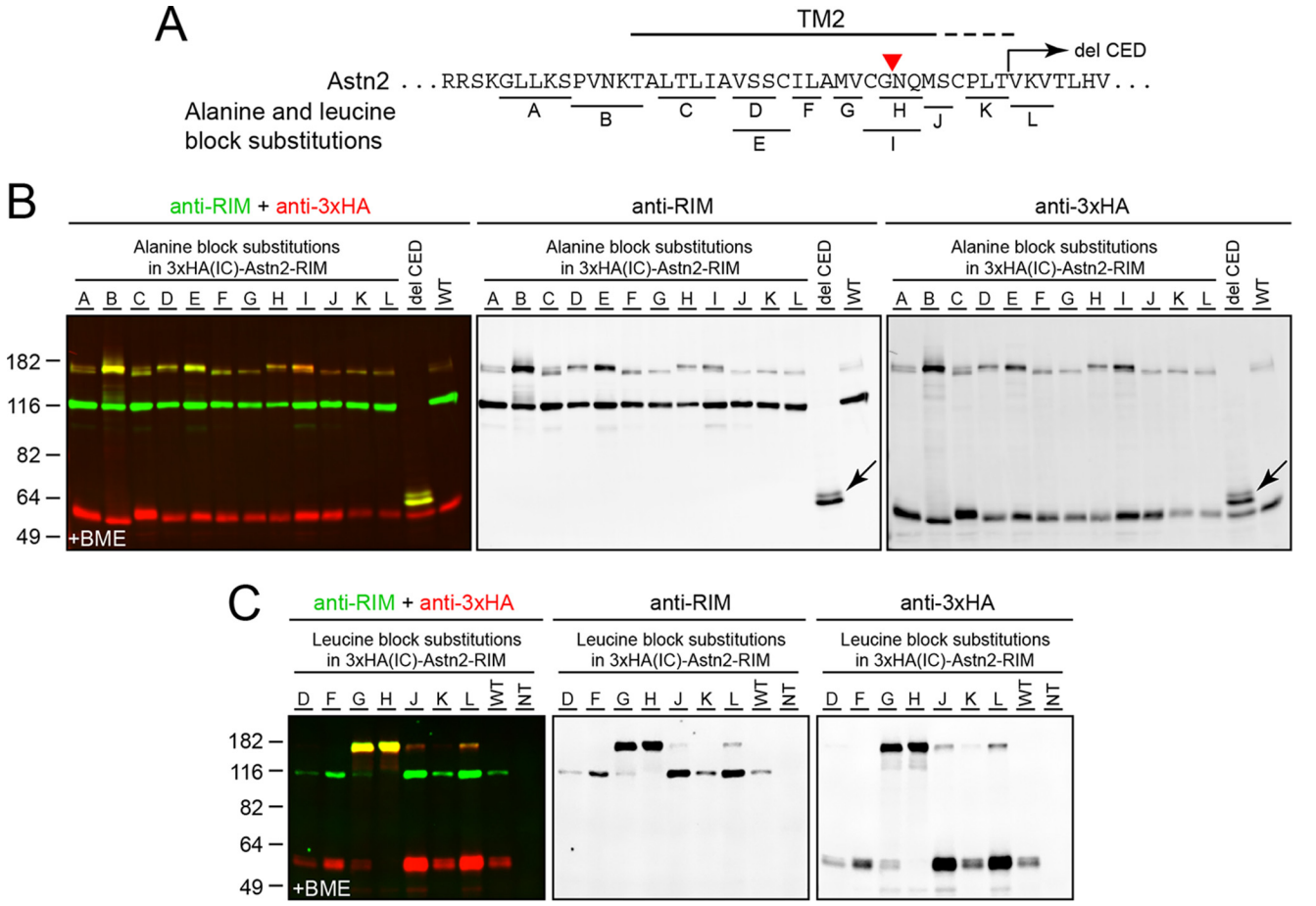

FIGURE 6. **Defining sequence requirements for proteolysis with alanine and leucine block substitutions in Astn2 TM2.** *A*, locations of alanine and leucine block substitutions and the deletion of the carboxyl-terminal ectodomain (*del CED*) in 3×HA(IC)-Astn2-RIM. For each of the *horizontal lines* labeled *A–L*, all of the amino acids above the *line* were changed to alanine. Additionally, for *horizontal lines D*, *F–H*, and *J–L*, all of the amino acids above the *line* were changed to leucine. The region encompassed by TM2, as predicted from the hydropathy profile, is indicated above. *Red arrowhead*, site of TM2 cleavage. *B*, anti-RIM and anti-3×HA immunoblots of alanine block substitutions and del CED in 3×HA(IC)-Astn2-RIM produced in transfected HEK293T cells. *Arrows* indicate that del CED is efficiently cleaved in TM2. *C*, anti-RIM and anti-3×HA immunoblots of leucine block substitutions in 3×HA(IC)-Astn2-RIM produced in transfected HEK293T cells.

altered the electrophoretic mobility of the resulting fragments (Fig. 6*B*).

To engineer a potentially more severe perturbation of TM2, we constructed an analogous set of leucine block substitutions, reasoning that the active site of the relevant intramembrane protease might be able to accommodate smaller side chains but not larger ones at some substrate positions. The leucine series showed a dramatic inhibition of cleavage when the substitution block encompassed the cleavage site or was several amino acids upstream of that position, but there was little or no effect of leucine substitution at other locations within TM2 (Fig. 6*C*). A deletion of the entire carboxyl-terminal ectodomain reduced the efficiency of TM2 cleavage but did not eliminate it (Fig. 6*A* and *arrows* in Fig. 6*B*). In these and other Astn2 mutants, there is no correlation between cleavage efficiency and steady state levels of Astn2.

As an additional test of substrate recognition, transmembrane segments from different type 1 and type 2 proteins were substituted for TM2 of Astn2 (Fig. 7). Replacement of TM2 by the transmembrane domain of CD4 (a type 1 membrane protein; Ref. 21) or by the transmembrane domain of the asialoglycoprotein receptor or the transferrin receptor (both type 2 transmembrane proteins; Refs. 22–24) eliminated cleavage in transfected HEK293T cells. Cleavage was also eliminated by replacement of TM2 with 21 leucines, but it was still observed—albeit at reduced efficiency—when TM2 was replaced by 21 alanines (*right arrow* in Fig. 7*C*). Interestingly, efficient cleavage was observed when TM2 was replaced by the transmembrane domain of CD74/Invariant chain (a type 2 transmembrane protein; Ref. 25; *left arrow* in Fig. 7*C*).

Transferrin receptor and CD74 are known substrates for SPPL-catalyzed intramembrane proteolysis, but such cleavage normally occurs only after removal of most of the carboxyl-terminal ectodomain (26–29). To our knowledge, intramembrane cleavage of the Asialoglycoprotein receptor has not been reported.

For the Astn2 derivatives with the CD74 transmembrane domain or 21 alanines in place of TM2, the amino-terminal fragment is under-represented on the immunoblot in Fig. 7*C*, suggesting that the presence of foreign sequences in place of TM2 may inhibit interchain disulfide bond formation and/or favor dissociation of amino- and carboxyl-terminal fragments leading to the selective degradation of the amino-terminal fragment. For those Astn2 derivatives with reduced TM2 cleavage,

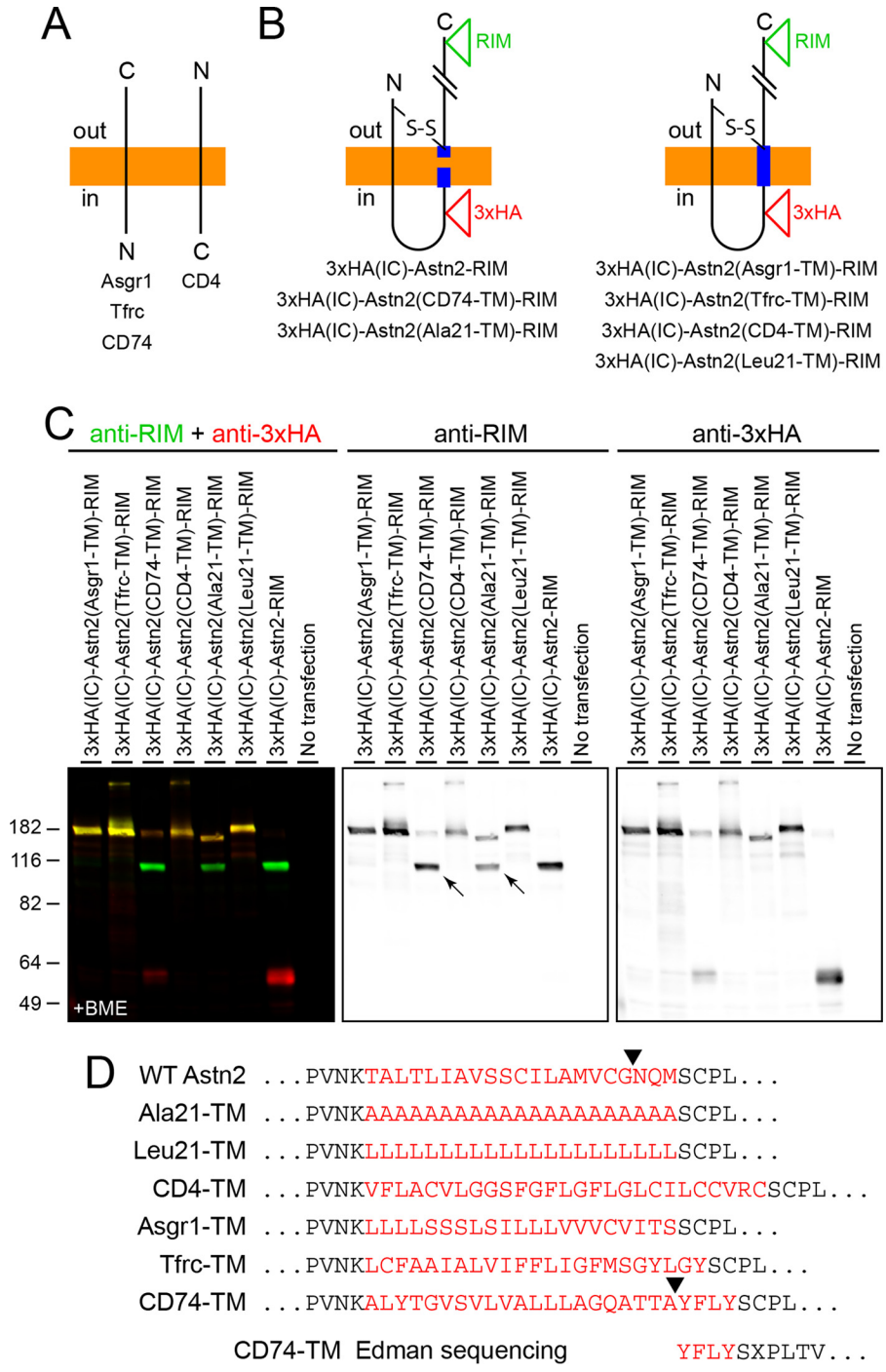

FIGURE 7. **Exchanging Astn2 TM2 for natural or synthetic transmembrane domains.** *A*, *left panel*, diagrams of asialoglycoprotein receptor (*Asgr1*), transferrin receptor (*Tfrc*), and CD74. *Right panel*, CD4 with amino and carboxyl termini labeled to indicate transmembrane topology. *B*, diagrammatic summary of TM2 cleavage or lack of cleavage based on the results in *C*. *C*, anti-RIM and anti-3×HA immunoblots of 3×HA(IC)-Astn2-RIM derivatives produced in transfected HEK293T cells. *Arrows* indicate Astn2 derivatives with efficient TM2 cleavage. *D*, sequences in and adjacent to Astn2 TM2 showing (in *red*) the region that was replaced in the transmembrane substitution derivatives. Amino-terminal Edman sequencing of the immunoaffinity-purified carboxyl-terminal fragment of 3×HA(IC)-Astn2(CD74-TM)-RIM is shown at the *bottom*, and the site of cleavage is indicated for this sequence and for WT 3×HA(IC)-Astn2-RIM by *black arrowheads*. The cleavage site amino-terminal to YFLY... in 3×HA(IC)-Astn2(CD74-TM)-RIM is centered in the cluster of transmembrane cleavage sites identified by mass spectrometry for CD74 expressed in HEK293 (see Fig. 2*B*, *left panel*, in Ref. 42).

the experiments described thus far do not rule out the possibility that trafficking of the Astn2 derivatives was altered, thereby decreasing its co-localization with the relevant intramembrane protease(s). As one test of this possibility, the plasma membrane localization of the seven leucine block substitution mutants (Fig. 6*C*) and the six substitutions of the entire length of TM2 (Fig. 7*C*) was assessed by immunostaining for the RIM epitope in intact transfected HEK293 cells (supplemental Fig. S3). This analysis shows that a similar fraction of the Astn2 proteins is present at the plasma membrane for these 13 mutants and for WT Astn2, suggesting that all of the mutant proteins can traverse the ER to Golgi to plasma membrane

pathway with roughly the same efficiency as WT Astn2. We conclude that gross mislocalization of the mutant Astn2 proteins—for example, retention in the ER caused by misfolding—cannot explain the failure of TM2 cleavage in a subset of the mutants.

The Astn2 derivative in which TM2 was replaced by the CD74 transmembrane domain was immunoaffinity-purified with mAb Rim3F4, and the carboxyl-terminal fragment was subjected to Edman sequencing. The resulting amino-terminal sequence, YFLYS*X*PTV, places the site of intramembrane cleavage at the same or nearly the same position as observed for native Astn2 (Fig. 7*D*). Edman sequencing of the carboxyl-terminal fragment of the Astn2 derivative in which TM2 was replaced by 21 alanines produced alanine signals over the first several sequencing cycles but did not produce clear sequences beyond that point, implying only that the cleavage occurred within the stretch of 21 alanines.

To assess the sufficiency of Astn2 TM2 as a substrate for intramembrane proteolysis, these sequences were inserted in place of the single transmembrane domain of two type 2 membrane proteins: the asialoglycoprotein receptor and CD74, each of which had been modified to also carry an amino-terminal RIM tag and a carboxyl-terminal 3×HA tag (Fig. 8, *A* and *B*). In control experiments, expression of doubly epitope-tagged Asialoglycoprotein receptor and CD74 in HEK293T cells was observed to produce the expected full-length products as assessed by immunoblotting for each tag (Fig. 8*C*). Insertion of Astn2 TM2 in place of the endogenous transmembrane domain in these proteins resulted in the appearance of a novel carboxyl-terminal fragment in the anti-3×HA immunoblot at a mobility corresponding to a reduction of ~8–10 kDa relative to the full-length proteins (*arrows* in Fig. 8*C*). This reduction is in good agreement with the 7–8-kDa reduction in size calculated for these proteins if we assume that cleavage occurs at the same TM2 site as observed in Astn2 (Fig. 8*A*). Attempts to visualize the ~7–8-kDa amino-terminal fragment by immunoblotting from 15% SDS/PAGE have been unsuccessful, suggesting that this fragment may be unstable (data not shown). Based on the appearance of the carboxyl-terminal fragment at substoichiometric abundance, the data suggest that the two chimeric proteins with Astn2 TM2 are substrates for intramembrane cleavage but with relatively low efficiency. Taken together, the block substitution and sequence swapping experiments demonstrate that Astn2 TM2 contains substantial substrate specificity, that sequences near the cleavage site likely play a steric role in permitting cleavage, that carboxyl-terminal extramembrane sequences enhance cleavage efficiency, and that a subset of natural or artificial transmembrane sequences can be cleaved if they are presented in the context of the Astn2 TM2 region.

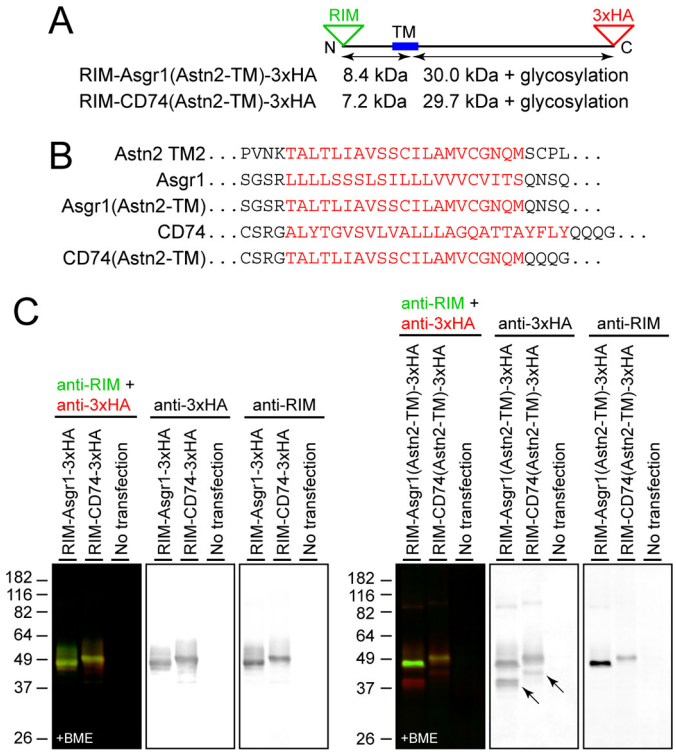

FIGURE 8. **Inserting Astn2 TM2 in place of the transmembrane regions of asialoglycoprotein receptor and CD74.** *A*, diagram of RIM- and 3×HA-tagged asialoglycoprotein receptor (*Asgr1*) and CD74 derivatives with Astn2 TM2, and the calculated molecular masses of amino- and carboxyl-terminal fragments generated by cleavage within TM2 between glycine and asparagine. *B*, transmembrane and flanking region sequences of Astn2, Asgr1, and CD74, and the TM2 replacement derivatives of Asgr1 and CD74. The sequences that were replaced or inserted are in *red*. *C*, anti-RIM and anti-3×HA immunoblots of RIM- and 3×HA-tagged asialoglycoprotein receptor (Asgr1) and CD74 (*left panel*) or their derivatives with Astn2 TM2 (*right panel*) produced in transfected HEK293T cells. *Arrows* indicate carboxyl-terminal cleavage products that are 7–8 kDa smaller than the full-length proteins.

Discussion

The experiments reported here establish an unusual transmembrane topology for Astn2, in which both the amino and carboxyl termini reside within the extracellular space (or, equivalently, the lumen of an internal membrane system) with a large connecting loop residing within the cytoplasm. Our experiments further identify intramembrane proteolytic cleavage in TM2 and a single disulfide bond linking the amino termini of the two resulting fragments. Proteolysis within TM2 occurs efficiently and is insensitive to conversion of some or all of the TM2 amino acids to alanine or to swapping of CD74 TM sequences for Astn2 TM2 sequences. In light of the high degree of sequence conservation between Astn1 and Astn2, their nearly identical hydropathy profiles, the Edman sequencing data showing that Astn1 TM2 is cleaved at a site that corresponds to the TM2 cleavage site in Astn2, and the virtually identical BME-dependent mobility shifts exhibited by Astn1 and Astn2, it is highly likely that Astn1 adopts the same transmembrane topology and covalent structure as defined here for Astn2.

Implications for Astrotactin Function—Astn2 gene deletions that encompass exon 5 modify the *Frizzled6*$^{-/-}$ hair orientation phenotype, and sequences from multiple Astn1 and Astn2 cDNA clones and from Astn2 RT-PCR products show that some mature astrotactin transcripts lack exon 4 (15). The present work shows that the amino acids encoded by exons 4 and 5 are part of the intracellular loop connecting TM1 and TM2 and that the absence of either or both exons (creating in-frame deletions in each case) has no effect on the proteolytic processing or yield of the resulting Astn2 variants in transfected cells. These data suggest that Astn2 variants lacking amino acids encoded by exon 4 and/or exon 5 may exhibit protein activity. Future

genetic experiments, including the construction of a definitive *Astn2* null allele, should be able to determine whether the genetic modifier activity of *Astn2* exon 5 deletion reflects an alteration of Astn2 function or a complete loss of Astn2 function.

The low electrophoretic mobility of Astn2 from mouse cerebellum in the absence of BME strongly implies the existence of a disulfide-linked partner. Identification of the putative partner could provide significant insights into Astn2 biogenesis and function.

Comparison with Proteolysis of Other Transmembrane Proteins—Proteolysis of transmembrane proteins can be either regulated or constitutive. An example of the former is the cholesterol-dependent cleavage of SREBPs by the site 1 protease and its partner, SCAP (SREBP cleavage-activating protein) (30). Examples of constitutive proteolysis in which the fragments remain associated, as they do for Astn2, include the cleavage of the insulin receptor, Lrp1 (low density lipoprotein-related receptor 1), and multiple members of the cell adhesion G-protein coupled receptor family (31–34). In each of these examples of constitutive proteolysis, cleavage occurs in the extracellular domain. For these proteins, and possibly for the astrotactins, proteolysis may facilitate or render irreversible a transition from an inactive to an active conformation. The high efficiency of astrotactin TM2 cleavage, together with the absence of any evidence for additional cleavage events beyond signal peptide removal, suggests that TM2 cleavage represents a constitutive step in astrotactin maturation, similar to the extracellular cleavage of insulin receptor or Lrp1.

Intramembrane cleavage is often dependent on or stimulated by an initial proteolytic cleavage outside of the membrane. It is also typically associated with the dissociation of the soluble and membrane-embedded proteolytic products. For example, the basic helix-loop-helix DNA-binding transcription factor domain of SREBP is released by intramembrane cleavage, which is catalyzed by site 2 protease only after an initial cleavage by site 1 protease of an extramembrane loop in SREBP (30). Similarly, the carboxyl-terminal cytoplasmic domain of Notch is released by intramembrane cleavage, which is catalyzed by γ-secretase after Notch-Jagged or Notch-Delta binding and subsequent extracellular domain cleavage by ADAM10 (A disintegrin and metalloprotease 10) (35–37). By contrast, intramembrane cleavage of astrotactins does not appear to require a second proteolytic cleavage, nor does it lead to dissociation of the two proteolytic products.

At present, the only known intramembrane proteases that cleave substrates with the type 2 topology of astrotactin TM2 are the site 2 protease and the SPP and SPPL peptidases (1, 6). Members of this family are highly conserved and are found in fungi, protozoa, plants, and animals (6). Studies of the substrate specificity of SPP and SPPL family members show that SPPLa and SPPL2b strongly favor substrates that have been subjected to ectodomain shedding, and SPP cleaves its signal peptide substrate following its release from the nascent polypeptide by signal peptidase (6, 19, 29, 38). However, SPPL3 makes an exception to this pattern by cleaving the first of two TM segments in the foamy virus envelope protein precursor in the absence of any other cleavage events (39). SPPL3 also cleaves the membrane anchoring segments of a wide variety of glycan-modifying enzymes in the Golgi apparatus (40, 41). Finally, recent studies of sequence determinants of transmembrane cleavage of CD74 by SPPL2a indicate that substrate specificity is determined by the combined effect of multiple residues in the CD74 transmembrane and juxtamembrane regions (42). Although the identity of the protease that cleaves the astrotactins remains to be determined, the observation of highly efficient astrotactin cleavage suggests the possibility that this type of transmembrane cleavage may be more widespread than is currently appreciated.

Experimental Procedures

Plasmids and Antibodies—Rabbit anti-3×HA antiserum was raised against a fusion of bacteriophage T7 gene 10 protein and 3×HA. Rabbit anti-Astn2 antisera was raised against a pGEMEX gene10 fusion protein with mouse Astn2 amino acids 777–989 (KPDS . . . VEIR) that was produced as an inclusion body in *Escherichia coli*, solubilized in SDS sample buffer, and resolved by preparative SDS-PAGE. The resulting rabbit antiserum was used at 1:5000 for immunoblotting of mouse cerebellar membranes. Mouse mAb against RIM (Rim3F4) was prepared as an ascites (Ref. 43; the hybridoma was a kind gift of Dr. Robert Molday). All membrane protein cDNAs were from mouse. Astn2 full-length cDNA was cloned from mouse embryonic day 15.5 back skin using RT-PCR. Val^{73} and Ser^{74} were duplicated upon 3×HA insertion in the 3×HA(SP)-Astn2-RIM construct. Astn1 full-length cDNA was purchased from Thermo Scientific (accession no. BC094666, clone ID 30545499).

Transfection—Standard procedures were used to transfect plasmid DNA into HEK293T or COS7 cells grown in DMEM/F-12 medium with 10% bovine serum and penicillin/streptomycin. For each well of cells to be transfected in a 12-well tray, 0.5 μg of DNA was diluted in 50 μl of serum-free medium. 1.5 μl of FuGENE® HD reagent (Promega) was added into the diluted DNA solution, mixed gently, and incubated for 10 min at room temperature before adding to the cells. To harvest large amount of proteins for amino-terminal sequencing, PEI was used to transfect plasmid DNA into HEK293T cells in a 10-cm plate format. For each 10-cm plate of cells to be transfected, 35 μl of PEI (1 mg/ml at PH 2.5) and 10 μg of DNA were each diluted in 500 μl of serum-free medium, mixed together, and incubated for 10 min at room temperature before adding it to the cells. For all mammalian cell transfections, the cells were incubated for 48 h post-transfection before assaying for protein expression.

Immunofluorescence—For immunostaining of COS7 cells (Fig. 1*C*), 48 h after transfection, the cells were changed into cold culture medium containing primary antibodies and incubated for 1.5 h at 4 °C. The cells were then rinsed with cold culture medium once and fixed in 4% paraformaldehyde in PBS at 4 °C for 1 h. The cells were washed in PBS for 10 min three times, incubated in secondary antibodies in PBST (0.1% Triton X-100 in PBS) at room temperature for 1 h, washed in PBST for 10 min three times, and then mounted in Fluoromount G (EM Sciences). For immunostaining of fixed cells, 48 h after transfection, the cells were fixed in 4% paraformaldehyde in PBS at 4 °C for 1 h. The cells were then washed in PBS for 10 min three

times, blocked with PBST containing 5% goat serum at 4 °C for 1 h, and incubated with primary and secondary antibodies using the same protocol as for staining of live cells. Dilutions of primary antibodies were: 3×HA antiserum (JH5606, 1:10,000) and mAb Rim3F4 ascites (1:3000). Secondary antibodies were purchased from Invitrogen. Images were captured using a Zeiss SFM700 confocal microscope with Zen software.

For immunostaining of live HEK293T cells (supplemental Fig. S3), cells were grown on gelatin-coated coverslips in a 12-well plate and transfected with plasmids expressing the indicated Astn2 constructs. One day after transfection, the 12-well plates were cooled on ice, and the medium was replaced with ice-cold serum-free medium containing mouse Rim3F4 ascites (1:3000). After incubation for 1 h on ice, coverslips were washed three times with ice-cold PBS with 1 mM $MgCl_2$ and 1 mM $CaCl_2$ (PBSMC) for 5 min and then fixed for 30 min with ice-cold 4% fresh paraformaldehyde in PBSMC. After three washes in cold PBSMC over 30 min, the coverslips were stained with rabbit anti-3×HA anti-serum (JH5606, 1:5000) in PBSMC containing 0.3% Triton X-100 (PBSMCT) supplemented with 5% normal goat serum for 3 h on ice. The coverslips were washed three times with ice-cold PBSMCT over 30 min and then incubated with DAPI and Alexa Fluor 594-conjugated goat anti-mouse and Alexa Fluor 488 goat anti-rabbit secondary antibodies (Invitrogen) in PBSMCT with 5% normal goat serum at room temperature for 90 min, washed three times in PBSCT, and mounted in Fluoromount G.

Preparation of Mouse Cerebellar Membranes—Purification of membranes from mouse cerebella was performed essentially as described for purification of membranes from transfected HEK293T cells (44). In brief, cerebella from ~20 wild type mice at postnatal day 10 were dissected into 5 ml of ice-cold homogenization buffer (PBS, 250 mM sucrose, protease inhibitor mixture (Roche), 0.1 mM PMSF, and 1.25 mM EDTA), homogenized with a Polytron for 30 s, and centrifuged at 5000 rpm for 5 min in a microcentrifuge at 4 °C to pellet nuclei. The turbid supernatant was layered on a 4-ml shelf PBS with 1.15 M sucrose and centrifuged at 105,000 × *g* (24,000 rpm in an SW40 rotor) for 30 min at 4 °C. Concentrated membranes were collected from the top of the sucrose shelf and resolved by SDS-PAGE with or without added BME. The mice were handled and housed according to the approved Institutional Animal Care and Use Committee protocol MO13M469 of the Johns Hopkins Medical Institutions.

Gel Electrophoresis and Immunoblotting—Transfected cells were lysed with ice-cold RIPA buffer (50 mM Tris-HCl, pH 7.4, 150 mM NaCl, 1% Triton X-100 and 0.5% deoxycholate) supplemented with protease inhibitors (Roche, complete mini mixture tablets). The cell lysates were incubated at 4 °C for 1 h, followed by centrifugation at 10,000 × *g* for 5 min at 4 °C. The samples were resolved by SDS-PAGE on a 12.5, 10, or 7.5% gel. Immunoblots were incubated at 4 °C overnight in the primary antibodies: rabbit anti-3×HA antiserum (JH5604, 1:250,000) and/or mAb Rim3F4 ascites (3F4, 1:50,000); the blots were then incubated with Li-Cor fluorescent secondary antibodies. The only immunoblot processed by a different protocol is the one shown in Fig. 2*A*, where HRP-conjugated secondary antibody (Bio-Rad) was used, and the immunoreactive bands were visualized with the SuperSignal West Pico Substrate (Pierce).

Amino-terminal (Edman) Sequencing—Protein G beads (20 μl of a 50% bead slurry) were coated with 5 μl of mAb Rim3F4 ascites at 4 °C for 1 h. 0.5 ml of transfected HEK293T cell lysate (~4 mg of protein) were incubated with Rim3F4 antibody-coated beads overnight at 4 °C. Beads with bound proteins were centrifuged at low speed and washed four times with cold RIPA buffer. 60 μl of Rim3F4 epitope peptide (NETYDLPLHPRTAG; Ref. 43) at 250 μg/ml in RIPA buffer was then added to the beads, which were gently vortexed at room temperature for 30 min to elute the RIM-tagged proteins. Eluted proteins were resolved on SDS-PAGE, transferred to PVDF membrane, and visualized by Coomassie Blue staining. Regions of interests were excised from the PVDF membrane and amino-terminally sequenced with the Procise Protein Sequencing System (Applied BioSystems Model 492).

Reproducibility—The number of times that each experiment was performed is listed in supplemental Table S1.

Author Contributions—H. C. and J. N. designed experiments. P. M. S. constructed many of the plasmids. J. W. produced anti-Astn2 antisera. H. C. conducted the experiments. H. C. and J. N. wrote the paper.

Acknowledgments—We thank Jodie Franklin of the Johns Hopkins Synthesis and Sequencing Facility for performing the amino-terminal Edman degradation, Amir Rattner for assistance with confocal microscopy, Sin Urban for advice on intramembrane proteolysis, Tao Ni and Robert Gilbert for advice on astrotactin structure, and Amir Rattner and Sin Urban for helpful comments on the manuscript.

References

1. Golde, T. E., Wolfe, M. S., and Greenbaum, D. C. (2009) Signal peptide peptidases: a family of intramembrane-cleaving proteases that cleave type 2 transmembrane proteins. *Semin. Cell Dev. Biol.* **20,** 225–230
2. Chen, G., and Zhang, X. (2010) New insights into S2P signaling cascades: regulation, variation, and conservation. *Protein Sci.* **19,** 2015–2030
3. Urban, S., and Dickey, S. W. (2011) The rhomboid protease family: a decade of progress on function and mechanism. *Genome Biol.* **12,** 231
4. Jurisch-Yaksi, N., Sannerud, R., and Annaert, W. (2013) A fast growing spectrum of biological functions of γ-secretase in development and disease. *Biochim. Biophys. Acta* **1828,** 2815–2827
5. Manolaridis, I., Kulkarni, K., Dodd, R. B., Ogasawara, S., Zhang, Z., Bineva, G., O'Reilly, N., Hanrahan, S. J., Thompson, A. J., Cronin, N., Iwata, S., and Barford, D. (2013) Mechanism of farnesylated CAAX protein processing by the intramembrane protease Rce1. *Nature* **504,** 301–305
6. Voss, M., Schröder, B., and Fluhrer, R. (2013) Mechanism, specificity, and physiology of signal peptide peptidase (SPP) and SPP-like proteases. *Biochim. Biophys. Acta* **1828,** 2828–2839
7. Fishell, G., and Hatten, M. E. (1991) Astrotactin provides a receptor system for CNS neuronal migration. *Development* **113,** 755–765
8. Zheng, C., Heintz, N., and Hatten, M. E. (1996) CNS gene encoding astrotactin, which supports neuronal migration along glial fibers. *Science* **272,** 417–419
9. Price, M., Lang, M. G., Frank, A. T., Goetting-Minesky, M. P., Patel, S. P., Silviera, M. L., Krady, J. K., Milner, R. J., Ewing, A. G., and Day, J. R. (2003) Seven cDNAs enriched following hippocampal lesion: possible roles in neuronal responses to injury. *Brain Res. Mol. Brain Res.* **117,** 58–67
10. Wilson, P. M., Fryer, R. H., Fang, Y., and Hatten, M. E. (2010) Astn2, a novel member of the astrotactin gene family, regulates the trafficking of ASTN1 during glial-guided neuronal migration. *J. Neurosci.* **30,** 8529–8540

11. Adams, N. C., Tomoda, T., Cooper, M., Dietz, G., and Hatten, M. E. (2002) Mice that lack astrotactin have slowed neuronal migration. *Development* **129,** 965–972
12. Vrijenhoek, T., Buizer-Voskamp, J. E., van der Stelt, I., Strengman, E., Genetic Risk and Outcome in Psychosis (GROUP) Consortium, Sabatti, C., Geurts van Kessel, A., Brunner, H. G., Ophoff, R. A., Veltman, J. A. (2008) Recurrent CNVs disrupt three candidate genes in schizophrenia patients. *Am. J. Hum. Genet.* **83,** 504–510
13. Glessner, J. T., Wang, K., Cai, G., Korvatska, O., Kim, C. E., Wood, S., Zhang, H., Estes, A., Brune, C. W., Bradfield, J. P., Imielinski, M., Frackelton, E. C., Reichert, J., Crawford, E. L., Munson, J., *et al.* (2009) Autism genome-wide copy number variation reveals ubiquitin and neuronal genes. *Nature* **459,** 569–573
14. Lionel, A. C., Tammimies, K., Vaags, A. K., Rosenfeld, J. A., Ahn, J. W., Merico, D., Noor, A., Runke, C. K., Pillalamarri, V. K., Carter, M. T., Gazzellone, M. J., Thiruvahindrapuram, B., Fagerberg, C., Laulund, L. W., Pellecchia, G., *et al.* (2014) Disruption of the ASTN2/TRIM32 locus at 9q33.1 is a risk factor in males for autism spectrum disorders, ADHD and other neurodevelopmental phenotypes. *Hum. Mol. Genet.* **23,** 2752–2768
15. Chang, H., Cahill, H., Smallwood, P. M., Wang, Y., and Nathans, J. (2015) Identification of astrotactin2 as a genetic modifier that regulates the global orientation of mammalian hair follicles. *PLoS Genet.* **11,** e1005532
16. Ni, T., Harlos, K., and Gilbert, R. (2016) Structure of astrotactin-2: a conserved vertebrate-specific and perforin-like membrane protein involved in neuronal development. *Open Biol.* **6,** 160053
17. Sun, H., Molday, R. S., and Nathans, J. (1999) Retinal stimulates ATP hydrolysis by purified and reconstituted ABCR, the photoreceptor-specific ATP-binding cassette transporter responsible for Stargardt disease. *J. Biol. Chem.* **274,** 8269–8281
18. Lemberg, M. K., and Martoglio, B. (2002) Requirements for signal peptide peptidase-catalyzed intramembrane proteolysis. *Mol. Cell* **10,** 735–744
19. Martin, L., Fluhrer, R., and Haass, C. (2009) Substrate requirements for SPPL2b-dependent regulated intramembrane proteolysis. *J. Biol. Chem.* **284,** 5662–5670
20. Fluhrer, R., Martin, L., Klier, B., Haug-Kröper, M., Grammer, G., Nuscher, B., and Haass, C. (2012) The α-helical content of the transmembrane domain of the British dementia protein-2 (Bri2) determines its processing by signal peptide peptidase-like 2b (SPPL2b). *J. Biol. Chem.* **287,** 5156–5163
21. Parnes, J. R., and Hunkapiller, T. (1987) L3T4 and the immunoglobulin gene superfamily: new relationships between the immune system and the nervous system. *Immunol. Rev.* **100,** 109–127
22. Schneider, C., Owen, M. J., Banville, D., and Williams, J. G. (1984) Primary structure of human transferrin receptor deduced from the mRNA sequence. *Nature* **311,** 675–678
23. Zerial, M., Melancon, P., Schneider, C., and Garoff, H. (1986) The transmembrane segment of the human transferrin receptor functions as a signal peptide. *EMBO J.* **5,** 1543–1550
24. Drickamer, K. (1987) Membrane receptors that mediate glycoprotein endocytosis: structure and biosynthesis. *Kidney Int. Suppl.* **23,** S167–S183
25. Stumptner-Cuvelette, P., and Benaroch, P. (2002) Multiple roles of the invariant chain in MHC class II function. *Biochim. Biophys. Acta* **1542,** 1–13
26. Beisner, D. R., Langerak, P., Parker, A. E., Dahlberg, C., Otero, F. J., Sutton, S. E., Poirot, L., Barnes, W., Young, M. A., Niessen, S., Wiltshire, T., Bodendorf, U., Martoglio, B., Cravatt, B., and Cooke, M. P. (2013) The intramembrane protease Sppl2a is required for B cell and DC development and survival via cleavage of the invariant chain. *J. Exp. Med.* **210,** 23–30
27. Bergmann, H., Yabas, M., Short, A., Miosge, L., Barthel, N., Teh, C. E., Roots, C. M., Bull, K. R., Jeelall, Y., Horikawa, K., Whittle, B., Balakishnan, B., Sjollema, G., Bertram, E. M., Mackay, F., *et al.* (2013) B cell survival, surface BCR and BAFFR expression, CD74 metabolism, and CD8- dendritic cells require the intramembrane endopeptidase SPPL2A. *J. Exp. Med.* **210,** 31–40
28. Schneppenheim, J., Dressel, R., Hüttl, S., Lüllmann-Rauch, R., Engelke, M., Dittmann, K., Wienands, J., Eskelinen, E. L., Hermans-Borgmeyer, I., Fluhrer, R., Saftig, P., and Schröder, B. (2013) The intramembrane protease SPPL2a promotes B cell development and controls endosomal traffic by cleavage of the invariant chain. *J. Exp. Med.* **210,** 41–58
29. Zahn, C., Kaup, M., Fluhrer, R., and Fuchs, H. (2013) The transferrin receptor-1 membrane stub undergoes intramembrane proteolysis by signal peptide peptidase-like 2b. *FEBS J.* **280,** 1653–1663
30. Brown, M. S., and Goldstein, J. L. (1999) A proteolytic pathway that controls the cholesterol content of membranes, cells, and blood. *Proc. Natl. Acad. Sci. U.S.A.* **96,** 11041–11048
31. Hedo, J. A., Kahn, C. R., Hayashi, M., Yamada, K. M., and Kasuga, M. (1983) Biosynthesis and glycosylation of the insulin receptor. Evidence for a single polypeptide precursor of the two major subunits. *J. Biol. Chem.* **258,** 10020–10026
32. Herz, J., Kowal, R. C., Goldstein, J. L., and Brown, M. S. (1990) Proteolytic processing of the 600 kd low density lipoprotein receptor-related protein (LRP) occurs in a trans-Golgi compartment. *EMBO J.* **9,** 1769–1776
33. Alarcón, C., Cheatham, B., Lincoln, B., Kahn, C. R., Siddle, K., and Rhodes, C. J. (1994) A Kex2-related endopeptidase activity present in rat liver specifically processes the insulin proreceptor. *Biochem. J.* **301,** 257–265
34. Araç, D., Boucard, A. A., Bolliger, M. F., Nguyen, J., Soltis, S. M., Südhof, T. C., and Brunger, A. T. (2012) A novel evolutionarily conserved domain of cell-adhesion GPCRs mediates autoproteolysis. *EMBO J.* **31,** 1364–1378
35. van Tetering, G., van Diest, P., Verlaan, I., van der Wall, E., Kopan, R., and Vooijs, M. (2009) Metalloprotease ADAM10 is required for Notch1 site 2 cleavage. *J. Biol. Chem.* **284,** 31018–31027
36. Weber, S., Niessen, M. T., Prox, J., Lüllmann-Rauch, R., Schmitz, A., Schwanbeck, R., Blobel, C. P., Jorissen, E., de Strooper, B., Niessen, C. M., and Saftig, P. (2011) The disintegrin/metalloproteinase Adam10 is essential for epidermal integrity and Notch-mediated signaling. *Development* **138,** 495–505
37. Weber, S., and Saftig, P. (2012) Ectodomain shedding and ADAMs in development. *Development* **139,** 3693–3709
38. Kirkin, V., Cahuzac, N., Guardiola-Serrano, F., Huault, S., Lückerath, K., Friedmann, E., Novac, N., Wels, W. S., Martoglio, B., Hueber, A. O., and Zörnig, M. (2007) The Fas ligand intracellular domain is released by ADAM10 and SPPL2a cleavage in T-cells. *Cell Death Differ.* **14,** 1678–1687
39. Voss, M., Fukumori, A., Kuhn, P. H., Künzel, U., Klier, B., Grammer, G., Haug-Kröper, M., Kremmer, E., Lichtenthaler, S. F., Steiner, H., Schröder, B., Haass, C., and Fluhrer, R. (2012) Foamy virus envelope protein is a substrate for signal peptide peptidase-like 3 (SPPL3). *J. Biol. Chem.* **287,** 43401–43409
40. Voss, M., Künzel, U., Higel, F., Kuhn, P. H., Colombo, A., Fukumori, A., Haug-Kröper, M., Klier, B., Grammer, G., Seidl, A., Schröder, B., Obst, R., Steiner, H., Lichtenthaler, S. F., Haass, C., *et al.* (2014) Shedding of glycan-modifying enzymes by signal peptide peptidase-like 3 (SPPL3) regulates cellular *N*-glycosylation. *EMBO J.* **33,** 2890–2905
41. Kuhn, P. H., Voss, M., Haug-Kröper, M., Schröder, B., Schepers, U., Bräse, S., Haass, C., Lichtenthaler, S. F., and Fluhrer, R. (2015) Secretome analysis identifies novel signal peptide peptidase-like 3 (Sppl3) substrates and reveals a role of Sppl3 in multiple Golgi glycosylation pathways. *Mol. Cell. Proteomics* **14,** 1584–1598
42. Hüttl, S., Helfrich, F., Mentrup, T., Held, S., Fukumori, A., Steiner, H., Saftig, P., Fluhrer, R., and Schröder, B. (2016) Substrate determinants of signal peptide peptidase-like 2a (SPPL2a)-mediated intramembrane proteolysis of the invariant chain CD74. *Biochem. J.* **473,** 1405–1422
43. Illing, M., Molday, L. L., and Molday, R. S. (1997) The 220-kDa rim protein of retinal rod outer segments is a member of the ABC transporter superfamily. *J. Biol. Chem.* **272,** 10303–10310
44. Nathans, J. (1990) Determinants of visual pigment absorbance: identification of the retinylidene Schiff's base counterion in bovine rhodopsin. *Biochemistry* **29,** 9746–9752